Multi-Parametric Model of the Heart from CT Images to Guide Ventricular Tachycardia Ablation

Sofia Antunes[1,2], Daniele Tresoldi[2], Caterina Colantoni[3], Anna Palmisano[3], Antonio Esposito[3], Sebastiano Colombo[4], Giuseppe Maccabelli[4], Paolo della Bella[4], Sergio Cerutti[1], Giovanna Rizzo[2]

[1]Department of Electronics, Information and Bioengineering, Politecnico di Milano, Milan, Italy
[2]Institute of Molecular Bioimaging and Physiology-CNR, Segrate, Italy
[3]Department of Radiology, Scientific Institute H. S. Raffaele, Milan, Italy
[4]Arrhythmia Department and Clinical Electrophysiology Laboratories, Scientific Institute H. S. Raffaele, Milan, Italy

Abstract

The purpose of this work was to construct a 3D multi-parametric model of the heart by automatically segmenting cardiac cavities, left myocardium, scar and epicardial fat from multidetector computed tomographic (MDCT) volumes, using a level set algorithm based on a new multi-scale stopping function. This method was applied to 4 patients with recurrent ventricular tachycardia (VT) undergoing contrast enhanced (CE)-MDCT imaging, composed by an angiographic (ANGIO) and a late enhanced (LE) scan, before electro-anatomic mapping (EAM) and radiofrequency ablation (RFa). The segmented structures were integrated into the clinical surgery software system (CARTO). The adequacy of our model was verified by an expert radiologist and an arrhythmologist using a qualitative score.

1. Introduction

In ventricular tachycardia (VT) ablation procedures, the exact location and extent of myocardial scar is important to decide whether the procedure will be epicardial or endocardial, as well as to reduce intervention time [1]. Today, contrast enhanced magnetic resonance imaging (CE-MRI) is considered the standard for the assessment of scar tissue. However, contrast enhanced multidetector computed tomographic (CE-MDCT) imaging could be an interesting alternative, since it is less prone to artefacts introduced by the metallic cardioverter usually implanted in these patients [2]. The tissue characterization capabilities of both imaging modalities are similar: in the same way as MRI, MDCT shows myocardium scar as delayed hyperenhanced zones (regions of increased signal intensity compared with normal myocardium zones), i.e. reduced outflow rates with respect to normal myocardium [3]. Moreover, in an acquisition, during one apnea, MDCT presents a higher spatial resolution compared to MRI, that is important in applications such as ablation surgeries which need a good 3D reconstruction of the heart structures.

In the identification of scar during substrate mapping, the presence and thickness of epicardial fat has also been shown to be of key importance, because it presents voltage characteristics similar to scar tissue and is often confused with scar [1]. Despite MDCT can reliably visualize epicardial fat distribution, it is nowadays neglected in the ablation procedures because fat needs a very time consuming manual segmentation of MDCT images.

In this work, we construct a multi-parametric model of the heart, containing anatomical information useful for guidance during VT ablation procedures. This model is obtained segmenting automatically left ventricle, right ventricle, myocardium, scar and epicardial fat.

2. Methods

In the following we present the pre-procedural MDCT acquisition and processing steps used to construct the multi-parametric heart model.

2.1. Study protocol

4 patients with recurrent VT underwent 64-slice-MDCT before electro-anatomic mapping (EAM) and radiofrequency ablation (RFa), including angiographic (ANGIO) and low-energy (80 kV) late enhanced (LE) scan, 10 minutes after high-concentration iodine injection. 3 out of 4 patients have an implantable cardioverter defibrillator (ICD). The voxel size of both scans is 0.4 x 0.4 x 0.4 mm.

EAM/RFa approach (endocardial or epicardial) was

chosen based on the prevalent distribution of scars at LE-MDCT.

2.2. ANGIO/LE scans registration

Although ANGIO and LE scans were acquired with a few minutes distance, misalignment of the patient between both scans often occurred as seen in Fig.1, which required registration.

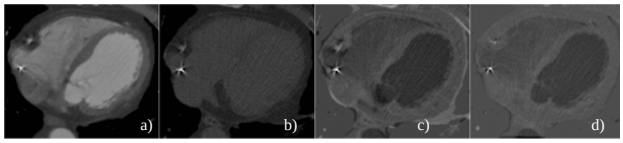

Figure 1. a) ANGIO scan, b) LE scan, c) subtraction of both scans and d) subtraction after affine registration.

To define the transformation T that align two different volumes we used an affine transformation with 12 degrees of freedom:

$$\begin{pmatrix} x' \\ y' \\ z' \end{pmatrix} = \begin{pmatrix} Tx \\ Ty \\ Tz \end{pmatrix} + \begin{pmatrix} Ta_{11} & Ta_{12} & Ta_{13} \\ Ta_{21} & Ta_{22} & Ta_{23} \\ Ta_{31} & Ta_{32} & Ta_{33} \end{pmatrix} \begin{pmatrix} x \\ y \\ z \end{pmatrix}$$

where the first matrix on the right side denotes the directional translations and the second vector contains the rotation, scaling and shearing information. The similarity metric used was the normalized mutual information [4], combination of the marginal and joint entropies of the images. The transformation model was estimated with the Powell's optimization method [5].

2.3. Segmentation

Both scans were firstly cropped to enclose only the heart volume.

2.3.1. Method

The segmentation model is a boundary-based geodesic active contour [6], where the embedded surface in the level set function can be formulated by the following partial differential equation:

$$\phi_t = cg(I)K|\nabla\phi| - bg(I)|\nabla\phi| - a\nabla g \cdot \nabla\phi$$

where the speed function includes a dependence on the curvature *c*, the propagation term *b*, and the advection term *a*. The edge stopping function *g* is based on a multi-scale approach, with the form:

$$g_n = \frac{1}{1 + e^{\left(\frac{I * h_n - \beta_n}{0.1}\right)}}, \text{ with } n = 1,2$$

where *h* and β change after convergence. h_1 and h_2 are the maximum responses of the two bi-dimensional bar filters, and the values of $\beta 1$ and $\beta 2$ are constants. The method is described in more detail in [7].

2.3.2. Anatomy extraction

On the angiographic scan, we re-sampled the volume into the short axis view and, to reduce signal to noise ratio maintaining boundary information, we applied an anisotropic diffusion smoothing [8].

After anisotropic filtering, we extracted two slices at 25% and 50% of the cropped heart volume, and used a Fuzzy C Mean algorithm to segment each of the two slices in 5 labels. On the label correspondent to the LV we identified the centroid on both slices and used these points as seeds for a 3D region growing algorithm. We summed the segmentations resulting from the region growing process of each seed point and used them as our active contour initialization. After contour propagation we obtained the LV structure. To obtain the myocardium contour initialization, the previous extracted structure was dilated and the operation of convex hull applied.

Finally, we joined myocardium and RV segmentation, computed the correspondent convex hull operation and used it as initialization for the active contour propagation to obtain the segmentation of the epicardial fat. The cardiac structures segmentation are shown in Fig.2 for two exemplificative cases.

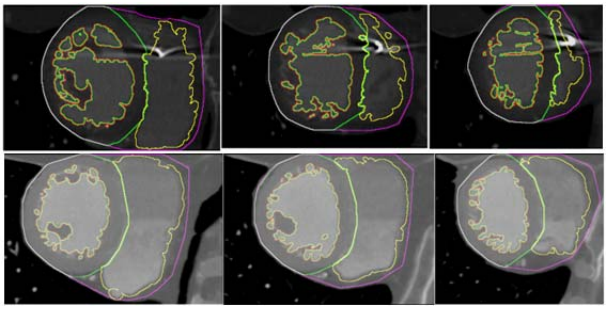

Figure 2. ANGIO scan overlaid with segmentations of anatomical structures in two different patients (the first has an ICD) and three different heart levels (basal, medial and apical). Artifacts of the ICD are visible on the first row.

2.3.3. Scar extraction

We aligned LE with respect to the ANGIO scan as described in Sec. 2.2, cropping the two datasets to exclude most ICD artefacts. After registration, and

because CE-MDCT had a very low signal to noise ratio, this scan was filtered using a Gaussian kernel. Using the MDCT LV segmentation as mask on the CE-MDCT scan, we calculated the mean vascular signal intensity as a segmentation threshold on this volume. Indeed, scar areas in the myocardium have an high signal intensity such as vascular structures. After thresholding, the volume is re-sampled into the short axis view, with the same parameters as the angiographic scan, and the MDCT myocardium segmentation was used as mask to include only myocardium areas of high SI. In patients with a metallic cardioverter, segmented areas near the ICD were excluded, because artefacts due to the metallic device also present high signal intensity. Two examples of scar segmentation results are shown in Fig. 3.

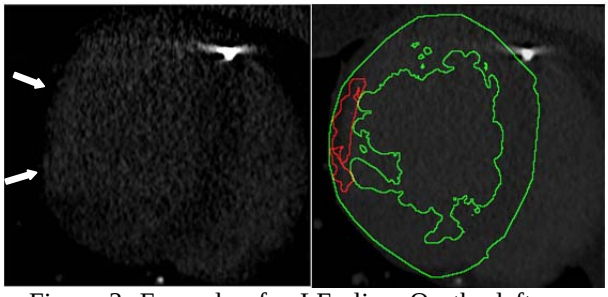

Figure 3. Example of a LE slice. On the left, arrows show scarred area and on the right LE overlaid with healthy (green) and scarred (red) myocardium from a patient.

3. Results

Segmentations of all cardiac structures were superimposed to the angiographic scan and, for each patient, LV, RV, myocardium and fat segmentations were evaluated on each of the 10 equal distributed slices by an expert radiologist. In the same way, scar segmentations were overlaid on the correspondent contrast enhanced scan and evaluated by the radiologist. The qualitative evaluation consists in the following 5-points classification: 1-unsatisfactory, 2-poor 3-satisfactory, 4-good, 5-excellent. The mean evaluation of all subjects is shown in Table 1.

Table 1. Mean qualitative evaluation of the segmented structures of the 4 patients with respect to pre-procedural CE-MDCT imaging.

Structure	Mean qualitative evaluation
LV	4
RV	4
myocardium	4
fat	3
scar	3

An example of the 3D reconstruction of the multi-parametric model of the heart is shown in Fig 4, where the reconstruction was done using surface rendering by implementing a marching cubes algorithm [9].

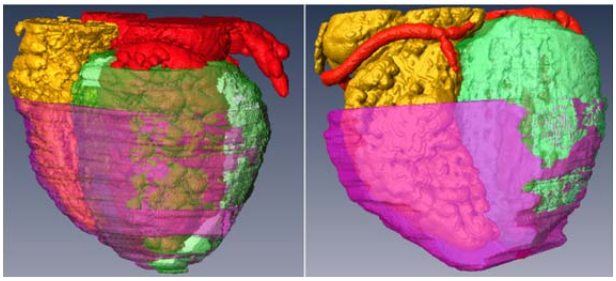

Figure 4. 3D reconstructions of the heart structures correspondent to two patients: yellow-RV, red-LV with coronaries, green- myocardium, white-scar and violet- fat. On the left, the patient has little fat layer, on the right side instead, there is a thick fat layer.

4. Discussion

Due to the technological development of MDCT in the last years, manual segmentation of such images is becoming an even less efficient option in the clinical practice. Today, model-based segmentation methods are widely used to segment cardiac structures [10-14]. However, they present some limitations on the LV and myocardium. In the former, papillary muscles were considered as LV cavity and in the latter, the substantial variation of wall thickness in such pathological subjects reduces their good performance. Therefore, it is usually still necessary to manually segment (or/and correct) the cardiac structures to plan adequately the ablation procedure. Additionally, to the best of our knowledge, there is no automatically segmentation method for epicardial fat and scar for ANGIO and LE images respectively, as proposed in this research.

In this work we demonstrated the feasibility of the automatic construction of an accurate heart model as an effective tool to assist the surgeon during ablation procedure. Main contributions of our work are the supply of a method that automatically segments all structures of interest and their integration in the clinical surgery software system to guide EAM and RFa procedures. The importance of our results are related to the reduction of the segmentation time and the optimization of intervention planning, being able, for example, to determine the fat layer thickness (crucial to plan a possible epicardial access).

The slight low evaluation of our segmentation for epicardial fat is principally due to the invisible pericardium in several zones and several slices. In the case of scar, the accurate segmentation is very limited to the low CE-MDCT resolution and the goodness of registration. The qualitative evaluation in the case of the

cardiac cavities and myocardium, were mostly influenced on the limited accurate segmentation near the ICD due to image artefacts that it generates (Fig. 2a and 3). In particular, if some scar is near to the ICD it cannot be detected using pre-procedural imaging modalities. Therefore, and despite the good judgment of the arrithmologist regarding the 3D reconstruction of the automatic scar segmentation as being very helpful and in good agreement with EAM during RFa procedure, at present, pre-procedural scar imaging remains only a complementation to EAM. This is evident in patients with ICD (very common in VT) in our study, and as shown in recent literature, also for patients without ICD [2].

Acknowledgements

The work was partially supported by the Italian Ministry of Health GR-2009-1594705. Sofia Antunes is grateful to the Portuguese Foundation for Science and Technology (FCT) by generous funding through the grant SFRH/BD/69488/2010.

References

[1] Piers SRD, van Taxis CFB, Tao Q, van der Geest RJ, Askar SF, Siebelink HJ, Zeppenfeld K. Epicardial substrate mapping for ventricular tachycardia ablation in patients with non-ischaemic cardiomyopathy: a new algorithm to differentiate between scar and viable myocardium developed by simultaneous integration of computed tomography and contrast-enhanced magnetic resonance imaging. Eur Heart J 2013; 34: 586-596.

[2] Dickfeld T, Tian J, Ahmad G, Jimenez A, Turgeman A, Kuk R, Peters M, Saliaris A, Saba M, Shorofsky S, Jeudy J. MRI-guided ventricular tachycardia ablation integration of late gadolinium-enhanced 3D scar in patients with implantable cardioverter-defibrillators. Circulation-Arrhythmia and Electrophysiology 2011; 4: 172-184.

[3] Gerber BL, Belge B, Legros GJ, Lim P, Poncelet A, Pasquet AS, Gisellu G, Coche E, Vanoverschelde JLJ. Characterization of acute and chronic myocardial infarcts by multidetector computed tomography - Comparison with contrast-enhanced magnetic resonance. Circulation 2006; 113: 823-833.

[4] Studholme C, Hill DLG, Hawkes DJ. An overlap invariant entropy measure of 3D medical image alignment. Pattern Recognit 1999; 32: 71-86.

[5] Pluim JPW, Maintz JBA, Viergever MA. Mutual-information-based registration of medical images: A survey. IEEE Trans. Med. Imaging 2003; 22: 986-100.

[6] Caselles V, Kimmel R, Sapiro G. Geodesic Active Contours. 1995.

[7] Antunes S, Colantoni C, Palmisano A, Esposito A, Cerutti S, Rizzo G. Automatic right ventricle segmentation in ct images using a novel multi-scale edge detector approach. Computing in Cardiology 2013.

[8] Perona P, Malik J. Scale-Space and Edge-Detection using Anisotropic Diffusion. IEEE Trans Pattern Anal Mach Intell 1990;12: 629-639.

[9] Schroeder W, Martin K, Lorensen B. The Visualization Toolkit 2nd edn. Upper Saddle River, NJ: Prentice-Hall, 2002.

[10] Ecabert O, Peters J, Walker MJ, Ivanc T, Lorenz C, von Berg J, Lessick J, Vembar M, Weese J. Segmentation of the heart and great vessels in CT images using a model-based adaptation framework. Med. Image Anal 2011; 15: 863-876.

[11] Peters J, Ecabert O, Meyer C, Kneser R, Weese J. Optimizing boundary detection via simulated search with applications to multi-modal heart segmentation. Med Image Anal 2010;14: 70-84.

[12] Kang D, Woo J, Slomka P J, Dey D, Germano G, Jay Kuo C. Heart chambers and whole heart segmentation techniques: review. Journal of Electronic Imaging 2012; 21: 010901-1.

[13] Kirisli HA, Schaap M, Klein S, Papadopoulou SL, Bonardi M, Chen CH, Weustink AC, Mollet NR, Vonken EJ, van der Geest RJ, van Walsum T, Niessen WJ. Evaluation of a multi-atlas based method for segmentation of cardiac CTA data: a large-scale, multicenter, and multivendor study. Med Phys 2010; 37: 6279-6291.

[14] Zheng Y, Barbu A, Georgescu B, Scheuering M, Comaniciu D. Four-chamber heart modeling and automatic segmentation for 3-D cardiac CT volumes using marginal space learning and steerable features. IEEE Trans Med Imaging 2008; 27: 1668-1681.

Address for correspondence.

Sofia Antunes
IBFM-CNR
Via Fratelli Cervi 93,
20090 Segrate (Milano), Italy
sofigantunes@gmail.com.